Arch Appl Mech (2015) 85:775–791
DOI 10.1007/s00419-015-0990-y

ORIGINAL

Carlos Cezar de La Plata Ruiz · José Luis L. Silveira

Mixed moving least-squares method for shakedown analysis

Received: 13 May 2014 / Accepted: 17 February 2015 / Published online: 28 February 2015

Abstract The elastic shakedown theory can be used to analyze and design structures under loads that change over time. Methods that use mixed interpolations provide simultaneous information regarding the kinematics and the equilibrium without the necessity of postprocessing. Meshless methods, as suggested by the name, do not require mesh generation or node connectivity and are an alternative to classical numerical methods. However, no current method exists that combines a mixed approximation of the kinematics and equilibrium with meshless methods for an elastic shakedown problem. In this paper, a discretization of a mixed variational principle for the elastic shakedown is presented based on the moving least-squares method, where stress and velocity approximation functions are used. The optimization problem, which comes from the mixed variational principle, determines the load factor and the residual stress and velocity fields. The stresses and velocities are approximated using linear and quadratic polynomial functions, respectively. The solution to the problem is obtained through a nonlinear algorithm based on Newton's method. The results obtained for the load factor and the residual stress field approach those obtained from the analytical solution for the tested examples.

Keywords Elastic shakedown · Moving least-squares method · Mixed interpolation · Variational principle

1 Introduction

Elastic shakedown theory has been used for the analysis and design of structures and machine elements subject to time-varying stress, such as beams [25], trusses [13], pipes, pressure vessels [6], welded pipes [21] and bearings and rails [9,26]. Shakedown studies have been conducted since 1920s [19]. The first contributions are due to Martin Grüning in 1926 and Hans Bleich in 1932 [35]. Melan [23] established a lower-bound shakedown theorem for continua. In 1956, Warner Koiter established a general kinematic theorem that provides an upper bound to the shakedown problem [18].

Due to its complexity, modeling of shakedown problems is generally completed using numerical methods. The most common numerical method for the discretization of the domains and structures analyzed in the shakedown problems is the finite element method. Stein et al. [29] provided the conditions for the shakedown

C. C. de La Plata Ruiz
Department of Mechanical Engineering, State University of Rio de Janeiro, Rio de Janeiro, Brazil
Tel.: +55 21 2334 0685
Fax: +55 21 2569 8631
E-mail: delaplataruiz@uol.com.br

J. L. L. Silveira (✉)
Department of Mechanical Engineering, Federal University of Rio de Janeiro, Rio de Janeiro, Brazil
Tel.: +55 21 3938 8378
Fax: +55 21 3938 8383
E-mail: jluis@mecanica.ufrj.br

of materials that present nonlinear kinematic hardening and, with the help of the finite element method, solved a number of shakedown problems. Garcea et al. [11], Nguyen-Xuan et al. [24] and Tran et al. [33] used the finite element method to analyze bi-dimensional structures subjected to a variable stress. Zouain and Silveira [41] presented mixed variational principles for the elastic shakedown and the incremental collapse and applied the finite element method to model a number of shakedown problems [28]. Despite its success, the finite element method, it is not the only known procedure for modeling shakedown problems.

Meshless methods are an alternative to the finite element method. These methods have the advantage of being implemented without requiring mesh generation or node connectivity, making them very attractive. Belytschko et al. [3] wrote one of the pioneering works on the application of meshless methods in engineering. This work numerically solved elasticity, fracture mechanics and heat conduction problems using a meshless method called the moving least-squares method. Despite computational implementation easiness, meshless methods have not been sufficiently investigated for the analysis of limit-state problems. Chen et al. [7] proposed the solution of elastic shakedown problems using the meshless local Petrov–Galerkin method. The paper presented a procedure that is based on an equilibrium principle to solve elastic shakedown problems for materials under kinematic hardening. Few papers exist that apply mixed interpolation to the elastic shakedown analysis. The advantages of applying mixed interpolation to numerical problems are the simultaneous kinematic and equilibrium results and the successful avoidance of locking [40]. However, methods do not yet exist for the elastic shakedown analysis that will permit the interpolation on a mixed form of kinematics and equilibrium using meshless methods. Therefore, the objectives of this paper are to present a methodology to solve shakedown problems that combines the computational efficiency of meshless methods, in particular, the moving least-squares method, with the advantages of a mixed variational principle, and to obtain solutions that will provide simultaneous results for equilibrium and kinematics.

2 Notation for kinematics, equilibrium and constitutive equations

V is the space of the velocity fields, and W is the space of the strain rate field. The velocity field, $\mathbf{v} \in V$, is kinematically compatible if the strain rate field, $\dot{\varepsilon} \in W$, is written as follows:

$$\dot{\varepsilon} = D\,\mathbf{v} \qquad \mathbf{v} \in V \quad \text{and} \quad \dot{\varepsilon} \in W \tag{1}$$

where D, based on the hypothesis of small strains, represents the strain tangent operator and is given by the symmetrical part of the gradient:

$$D = \frac{1}{2}\left(\nabla \cdot + \nabla^{\mathrm{T}} \cdot\right) \tag{2}$$

If W' is the space of the strain fields, then the field, $\mathbf{T} \in W'$, respects the equilibrium condition when the following relationship between the internal and external power is satisfied:

$$\int_B \mathbf{T} \cdot D\mathbf{v}\, dB = \int_B \mathbf{b} \cdot \mathbf{v}\, dB + \int_{\Gamma_\tau} \tau \cdot \mathbf{v}\, d\Gamma_\tau \quad \forall\, \mathbf{v} \in V \tag{3}$$

where B represents the region on $\mathbb{R}^3$ occupied by the body in question; Γ_τ indicates the part of the boundary of B where the surface forces, τ, are prescribed and $\mathbf{b}$ is the body force field.

The following notation will be adopted:

$$\langle \mathbf{T}, D\mathbf{v} \rangle = \int_B \mathbf{T} \cdot D\mathbf{v}\, dB \tag{4}$$

$$\langle F, \mathbf{v} \rangle = \int_B \mathbf{b} \cdot \mathbf{v}\, dB + \int_{\Gamma_\tau} \tau \cdot \mathbf{v}\, d\Gamma_\tau \tag{5}$$

The condition for a field, $\mathbf{T} \in W'$, to satisfy the equilibrium condition is reduced to the following:

$$\langle \mathbf{T}, D\mathbf{v} \rangle = \langle F, \mathbf{v} \rangle \quad \forall\, \mathbf{v} \in V \tag{6}$$

S is the set of stress fields, $\mathbf{T}$, that satisfy the equilibrium condition and is defined as follows:

$$S = \{\mathbf{T} \in W' \,|\, \langle \mathbf{T}, D\mathbf{v} \rangle = \langle F, \mathbf{v} \rangle \quad \forall\, \mathbf{v} \in V\} \tag{7}$$

A stress field, $\mathbf{T}^r$, in a body with a volume B, is said to be self-equilibrated or residual if it is in equilibrium with a null external load, F, as follows:

$$\langle \mathbf{T}^r, D\mathbf{v} \rangle = 0 \quad \forall\, \mathbf{v} \in V \tag{8}$$

The set of the self-equilibrated, or residual, stresses that act on a specific body is represented by S^r and given by [28]:

$$S^r = \{\mathbf{T}^r \in W' \big| \langle \mathbf{T}^r, D\mathbf{v} \rangle = 0 \quad \forall\, \mathbf{v} \in V\} \tag{9}$$

Consider $f(\mathbf{T})$ as a yield function for ideally plastic materials with associated plastic flow. If $f(\mathbf{T}) \leq 0$, then $\mathbf{T}$ is said to be plastically admissible and the set P of plastically admissible stress fields [39] is represented by:

$$P = \{\mathbf{T} \in W' \big| f(\mathbf{T}) \leq 0\} \tag{10}$$

A stress field that respects the equilibrium condition and that acts on a body that ideally responds elastically to any load is called an unlimited elastic stress field. Therefore, if the field, $\mathbf{T}^e$, is unlimitedly elastic, then the below is valid:

$$\langle \mathbf{T}^e, D\mathbf{v} \rangle = \langle F, \mathbf{v} \rangle \quad \forall\, \mathbf{v} \in V \tag{11}$$

One of the objectives of this paper is to determine at what point it is possible to amplify an elastic stress domain without the occurrence of body failure due to alternating plasticity or incremental collapse (ratcheting). Therefore, from ω, the maximum factor of unlimited elastic stress amplification, the amplified elastic stress, $\mathbf{T}^E$, can be determined from the following:

$$\mathbf{T}^E = \omega \mathbf{T}^e \tag{12}$$

In this paper, the stress field, $\mathbf{T}$, is calculated using a combination of two parcels: one elastic, $\omega\mathbf{T}^e$, and one residual, $\mathbf{T}^r$. The sum of the two parcels is the total stress (or total stress field) and given mathematically as follows:

$$\mathbf{T} = \omega \mathbf{T}^e + \mathbf{T}^r \tag{13}$$

Considering that a mechanically independent load quantity, α, acts on the body, then the load domain can be assumed to be formed by a convex polyhedron of m vertices, where $m = 2^\alpha$.

3 Variational principles for shakedown

The Bleich–Melan theorem establishes that a body or structure will adapt elastically to the variations of a load contained in a domain if, and only if, it exists a field of residual stress, $\mathbf{T}^r$, independent of the time and in such a way that its superposition to any stress, $\mathbf{T}^e$, belonging to the domain of varying elastic stress can be plastically admissible [42]. Based on this theorem, a static variational principle can be written that supplies the maximum load factor, ω, so that a residual stress field exists for which the structure will adapt. Therefore, the following optimization problem is established to determine the load factor, ω:

$$\omega = \sup_{\omega^*, \mathbf{T}^r} \omega^* \left| \begin{array}{l} \omega^* \mathbf{T}^{e\alpha} + \mathbf{T}^r \in P \quad \alpha = 1 \ldots m \\ \mathbf{T}^r \in S^r \end{array} \right. \tag{14}$$

A constraint is eliminated, and a mixed principle [43] is established in the previous static principle by introducing an exact penalty for the equilibrium [31]:

$$\omega = \sup_{\omega^*, \mathbf{T}^r} \left[\omega^* + \inf_{\mathbf{v}} \langle \mathbf{T}^r, D\mathbf{v} \rangle \right] \Big| \omega^* \mathbf{T}^{e\alpha} + \mathbf{T}^r \in P \quad \alpha = 1 \ldots m \tag{15}$$

or

$$\omega = \sup_{\omega^*, \mathbf{T}^r} \inf_{\mathbf{v}} \left[\omega^* + \langle \mathbf{T}^r, D\mathbf{v} \rangle \right] \Big| f(\omega^* \mathbf{T}^{e\alpha} + \mathbf{T}^r) \leq 0 \quad \alpha = 1 \ldots m \tag{16}$$

According to the Bleich–Melan theorem, the existence of a residual stress field is sufficient to ensure shakedown. Moreover, the residual stress field obtained through the variational principle (14) is nonunique

in the mathematical sense and does not necessarily match the actual field. The same statement applies to the residual stress fields obtained through the variational principle (16) and its discrete counterpart.

The variational principle (16) is now discretized using approximate functions for $\mathbf{T}^r$ and $\mathbf{v}$. Assuming that $\hat{\mathbf{T}}^r$ represents the approximate residual stress field and $\hat{\mathbf{v}}$ represents the approximate velocity field; then, it is possible to represent the residual stress tensor as a vector and to approximate the stress and velocity fields as follows:

$$\hat{\mathbf{T}}^r = \Psi T \tag{17}$$

$$\hat{\mathbf{v}} = \Phi v \tag{18}$$

where Ψ and Φ are matrices of the stress and velocity shape functions and T and v represent residual stress and velocity vectors at the base or nodal points.

Then, it is possible to write a discrete variational principle as follows:

$$\omega = \max_{\omega^*, \hat{\mathbf{T}}^r} \min_{\hat{\mathbf{v}}} \left[\omega^* + \int_B \hat{\mathbf{T}}^r \cdot D\hat{\mathbf{v}}\, dB \right] \Bigg| f(\omega^* \hat{\mathbf{T}}^{e\alpha} + \hat{\mathbf{T}}^r) \leq 0 \quad \alpha = 1 \ldots m \tag{19}$$

For the previous expression, $\hat{\mathbf{T}}^{e\alpha}$ represents an unlimited elastic stress field that can be either a numerically approximated field or an analytically obtained field.

Therefore, the discrete variational principle [43] can be written as follows:

$$\omega = \max_{\omega^*, T} \min_{v} \left[\omega^* + \int_B \Psi T \cdot D\Phi v\, dB \right] \Bigg| f(\omega^* T^{e\alpha} + T) \leq 0 \quad \alpha = 1 \ldots m \tag{20}$$

where T^e represents an elastic stress vector on the nodal points.

The numerical results are obtained with mixed approximation where the equilibrium is weak; hence, lower or upper bounding can not be assured [43]. It must be noted that

$$\int_B \Psi T \cdot D\Phi v dB = T \cdot \mathbf{B} v \tag{21}$$

where

$$\mathbf{B} = \int_B \Psi^{\mathrm{T}} D\Phi dB \tag{22}$$

Therefore, the optimization problem can be written as follows:

$$\omega = \max_{\omega^*, T} \min_{v} \left[\omega^* + T \cdot \mathbf{B} v \right] \Big| f(\omega^* T^{e\alpha} + T) \leq 0 \quad \alpha = 1 \ldots m \tag{23}$$

The elements of the matrix, $\mathbf{B}$, are composed of the stress shape functions and the derivative of the velocity shape functions. It is noted that $\mathbf{B}$ is constructed similarly to a mesh of mixed finite elements [5]. In this paper, the matrix $\mathbf{B}$ will be constructed from mixed moving least-squares meshless method, where both stress approximation and velocity approximation functions are used.

4 Mixed moving least-squares method

In the use of the conventional least-squares method, the coefficients of a polynomial function are obtained by minimizing the sum of squared errors in the base points. In the moving least-squares method, the approximating function is always a polynomial and its coefficients are obtained by minimizing the sum of squared errors in the base points, weighted by radial base functions.

Based on Belytschko et al. [4], each velocity component, $v_j(\mathbf{x})$, and each stress component, $T_k(\mathbf{x})$, in a generic point, $\mathbf{x}$, can be approximated as follows:

$$v_j(\mathbf{x}) = \sum_{i=1}^{m_v} p_{v_i}(\mathbf{x}) a_{v_i}(\mathbf{x}) \equiv \mathbf{p}_v{}^{\mathrm{T}}(\mathbf{x}) \mathbf{a}_v(\mathbf{x}) \qquad j = 1 \ldots n_v \tag{24}$$

$$T_k(\mathbf{x}) = \sum_{i=1}^{m_t} p_{t_i}(\mathbf{x}) a_{t_i}(\mathbf{x}) \equiv \mathbf{p}_t{}^{\mathrm{T}}(\mathbf{x}) \mathbf{a}_t(\mathbf{x}) \qquad k = 1 \ldots n_t \tag{25}$$

where

m_v and m_t are the number of monomials from the polynomial base used to approximate the velocities and the stresses, respectively;
n_v and n_t are, respectively, the number of degrees of freedom for the velocity and the number of components of stress, at the point $\mathbf{x}$;
$\mathbf{p}_v(\mathbf{x})$ is a vector composed of m_v monomials of a polynomial for the velocity approximation;
$\mathbf{a}_v(\mathbf{x})$ is a vector of m_v coefficients of the polynomial base of velocities;
$\mathbf{p}_t(\mathbf{x})$ is a vector composed of m_t monomials of a polynomial for the stress approximation;
and $\mathbf{a}_t(\mathbf{x})$ is a vector of m_t coefficients of the polynomial stress base.

Based on previous works on the development of the meshless method [1,3,15], it is possible to demonstrate that the value at a point $\mathbf{x}$ of the velocity shape function at the node i of the discretized domain is given by the following:

$$\phi_i(\mathbf{x}) = w(\|\mathbf{x} - \mathbf{x}_i\|)\, \mathbf{p}_v{}^{\mathrm{T}}(\mathbf{x}) \mathbf{A}_v^{-1}(\mathbf{x})\, \mathbf{p}_v(\mathbf{x}_i) \tag{26}$$

where

$\phi_i(\mathbf{x})$ is an element of the matrix Φ of the velocity shape functions [Eq. (18)];
$\|\mathbf{x} - \mathbf{x}_i\|$ is a scalar quantity given by the distance between the point $\mathbf{x}$ and the base point $\mathbf{x}_i$;
$w(\|\mathbf{x} - \mathbf{x}_i\|)$ is the weight function that is dependent on the distance between $\mathbf{x}$ and $\mathbf{x}_i$;
and $\mathbf{A}_v(\mathbf{x})$ is a $m_v \times m_v$ matrix given by the following:

$$\mathbf{A}_v(\mathbf{x}) = \sum_{i=1}^{n} w(\|\mathbf{x} - \mathbf{x}_i\|) \mathbf{p}_v(\mathbf{x}_i) \mathbf{p}_v^{\mathrm{T}}(\mathbf{x}_i) \tag{27}$$

In the previous expression, n is the number of base points or the number of nodal points.

Similarly, the stress shape functions can be written as follows:

$$\psi_i(\mathbf{x}) = w(\|\mathbf{x} - \mathbf{x}_i\|) \mathbf{p}_t^{\mathrm{T}}(\mathbf{x}) \mathbf{A}_t^{-1} \mathbf{p}_t(\mathbf{x}_i) \tag{28}$$

where $\psi_i(\mathbf{x})$ is an element of the matrix Ψ of the stress shape functions [Eq. (17)] and $\mathbf{A}_t(\mathbf{x})$ is an $m_t \times m_t$ matrix given by the following:

$$\mathbf{A}_t(\mathbf{x}) = \sum_{i=1}^{n} w(\|\mathbf{x} - \mathbf{x}_i\|) \mathbf{p}_t(\mathbf{x}_i) \mathbf{p}_t^{\mathrm{T}}(\mathbf{x}_i) \tag{29}$$

In the previous expressions, $\mathbf{x}$ represents a generic point with the coordinates (x, y, z). Therefore, $\mathbf{x}$ can be substituted with the spatial coordinates (x, y, z) or if in the plane, with the coordinates (x, y). To construct the matrix $\mathbf{B}$ for a plane problem, the derivatives of the velocity shape functions ϕ_i with respect to the coordinates x and y are required. The following notation will be used to manipulate the expressions that involve the partial derivatives with respect to x and y:

$$\frac{\partial}{\partial x} = (\cdot)_{,x} \quad \text{and} \quad \frac{\partial}{\partial y} = (\cdot)_{,y} \tag{30}$$

Therefore, the derivatives of the velocity shape functions are:

$$\phi_{i,x} = \mathbf{L}_{,x}\mathbf{E} + \mathbf{L}\mathbf{E}_{,x} \quad \text{and} \quad \phi_{i,y} = \mathbf{L}_{,y}\mathbf{E} + \mathbf{L}\mathbf{E}_{,y} \tag{31}$$

where $\mathbf{E}$ and its derivatives are given by the following:

$$\mathbf{E} = w(\|\mathbf{x} - \mathbf{x}_i\|)\mathbf{p}_v(\mathbf{x}_i) \tag{32}$$

$$\mathbf{E}_{,x} = w(\|\mathbf{x} - \mathbf{x}_i\|)_{,x}\mathbf{p}_v(\mathbf{x}_i) \quad \text{and} \quad \mathbf{E}_{,y} = w(\|\mathbf{x} - \mathbf{x}_i\|)_{,y}\mathbf{p}_v(\mathbf{x}_i) \tag{33}$$

In expressions (31), $\mathbf{L}$ and its derivatives are line matrices with m_v columns and $\mathbf{L}$ is defined as follows [10]:

$$\mathbf{L}(x, y) = \mathbf{p}_v^{\mathrm{T}}(x, y)\mathbf{A}_v^{-1} \tag{34}$$

The derivatives of $\mathbf{L}$ are given by the below:

$$\mathbf{L}_{,x} = \mathbf{p}_v^{\mathrm{T}}(x, y)_{,x}\mathbf{A}_v^{-1} + \mathbf{p}_v^{\mathrm{T}}(x, y)\mathbf{A}_{v,x}^{-1} \tag{35}$$

$$\mathbf{L}_{,y} = \mathbf{p}_v^{\mathrm{T}}(x, y)_{,y}\mathbf{A}_v^{-1} + \mathbf{p}_v^{\mathrm{T}}(x, y)\mathbf{A}_{v,y}^{-1} \tag{36}$$

where

$$\mathbf{A}_{v,x}^{-1} = -\mathbf{A}_v^{-1}\mathbf{A}_{v,x}\mathbf{A}_v^{-1} \quad \text{and} \quad \mathbf{A}_{v,y}^{-1} = -\mathbf{A}_v^{-1}\mathbf{A}_{v,y}\mathbf{A}_v^{-1} \tag{37}$$

with

$$\mathbf{A}_{v,x} = \mathbf{P}_v^{\mathrm{T}}\mathbf{G}_{,x}\mathbf{P}_v \quad \text{and} \quad \mathbf{A}_{v,y} = \mathbf{P}_v^{\mathrm{T}}\mathbf{G}_{,y}\mathbf{P}_v \tag{38}$$

The matrix $\mathbf{P}_v^{\mathrm{T}}$ is defined as follows [4]:

$$\mathbf{P}_v^{\mathrm{T}} = \begin{bmatrix} \mathbf{p}_v(x_1) & \mathbf{p}_v(x_2) & \mathbf{p}_v(x_3) & \dots & \mathbf{p}_v(x_n) \end{bmatrix} \tag{39}$$

Note that $\mathbf{P}_v^{\mathrm{T}}$ is an $n \times m_v$ matrix. Consequently, $\mathbf{P}_v$ is an $m_v \times n$ matrix.

In expressions (38), $\mathbf{G}_{,x}$ and $\mathbf{G}_{,y}$ represent $n \times n$ diagonal matrices of the derivative of the weight functions with respect to x and y, respectively, and $\mathbf{G}$ is an $n \times n$ diagonal matrix given by the following:

$$\mathbf{G} = \mathrm{diag}[w(\|\mathbf{x} - \mathbf{x}_i\|)] \tag{40}$$

In this paper, the radial base functions used were proposed by Wu [36]:

$$w(d) = (1 - d)^7(5 + 35d + 101d^2 + 147d^3 + 101d^4 + 35d^5 + 5d^6) \tag{41}$$

$$\frac{\partial w}{\partial d} = -78d + 572d^3 - 2574d^5 + 3003d^6 - 1287d^8 + 429d^{10} - 65d^{12} \tag{42}$$

In the previous expressions, d represents a normalized distance from a generic point to a base point.

For a node, i, the normalized distance, d_i, from a point $\mathbf{x}$ to the node $\mathbf{x}_i$ is given by the following:

$$d_i = \|\mathbf{x} - \mathbf{x}_i\| \tag{43}$$

or

$$d_i = \frac{1}{r}\sqrt{(x - x_i)^2 + (y - y_i)^2} \tag{44}$$

As observed in Sect. 3, expression (22), the matrix $\mathbf{B}$ is found by integrating over the body volume the product of the stress approximation matrix and a matrix of the derivatives of the velocity approximation functions.

For the plane case, the stress approximation matrix Ψ is given by the following:

$$\Psi = \begin{bmatrix} \psi_1 & 0 & 0 & \psi_2 & 0 & 0 & \dots & \psi_{n-1} & 0 & 0 & \psi_n & 0 & 0 \\ 0 & \psi_1 & 0 & 0 & \psi_2 & 0 & \dots & 0 & \psi_{n-1} & 0 & 0 & \psi_n & 0 \\ 0 & 0 & \psi_1 & 0 & 0 & \psi_2 & \dots & 0 & 0 & \psi_{n-1} & 0 & 0 & \psi_n \end{bmatrix} \tag{45}$$

where ψ_i is a function of x and y, and the matrix $D\Phi(x, y)$ is given by the following:

$$D\Phi = \begin{bmatrix} \phi_{1,x} & 0 & \phi_{2,x} & 0 & \phi_{3,x} & 0 & \phi_{4,x} & 0 & \dots & 0 \\ 0 & \phi_{1,y} & 0 & \phi_{2,y} & 0 & \phi_{3,y} & 0 & \phi_{4,y} & \dots & \phi_{n,y} \\ \phi_{1,y} & \phi_{1,x} & \phi_{2,y} & \phi_{2,x} & \phi_{3,y} & \phi_{3,x} & \phi_{4,y} & \phi_{4,x} & \dots & \phi_{n,x} \end{bmatrix} \tag{46}$$

The components of the matrix $\mathbf{B}$, which is $3n \times 2n$, can be obtained by numeric integration.

In the next section, the algorithm proposed by Zouain et al. [43] is applied to the solution of the optimization problem found using the mixed variational principle (20).

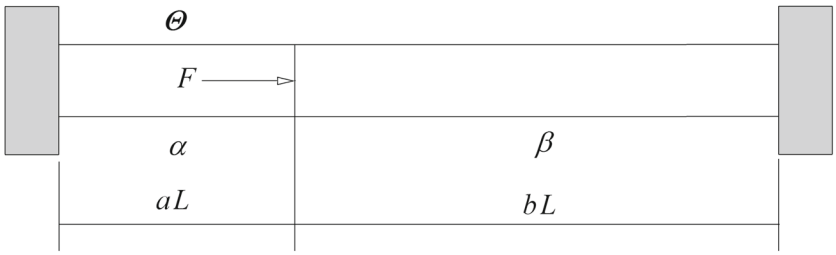

Fig. 1 Two bars were subjected to temperature and axial load variations

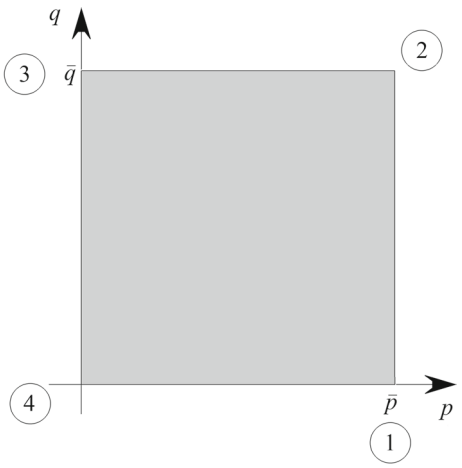

Fig. 2 Load polyhedron

5 Numeric results

In each one of the following examples, the solution of the optimization problem yields the loading factor, ω, the velocity field, v, and the residual stress field, T. The material is assumed elastic ideally plastic and satisfies the von Mises criterion.

5.1 Two bars of the same material were subjected to variable temperature and axial load

Two bars of length aL and bL are shown in Fig. 1. The first bar is called α, and the second is called β. The α bar is subjected to a variable axial load, F, and an independent temperature variation, Θ. Both bars have a transverse section area, A, the same material with a yield stress, Y_0, Young's modulus, E, and a thermal expansion coefficient, c. The load polyhedron acting on bar α is shown schematically in Fig. 2.

The elastic stress on the bars, α and β, and the load factor, ω, are given by the following expressions based on the work of Silveira and Zouain [28]:

$$T_\alpha^1 = 2b\,\bar{p}\,Y_0 \qquad T_\beta^1 = 2a\,\bar{p}\,Y_0 \tag{47}$$

$$T_\alpha^2 = (2b\,\bar{p} - a\,\bar{q})\,Y_0 \qquad T_\beta^2 = (-2a\,\bar{p} - a\,\bar{q})\,Y_0 \tag{48}$$

$$T_\alpha^3 = -a\,\bar{q}\,Y_0 \qquad T_\beta^3 = -a\,\bar{q}\,Y_0 \tag{49}$$

$$T_\alpha^4 = 0 \qquad T_\beta^4 = 0 \tag{50}$$

$$\omega = \frac{2}{2\bar{p} + a\bar{q}} \tag{51}$$

where $0 \le p \le \bar{p}$ and $0 \le q \le \bar{q}$.

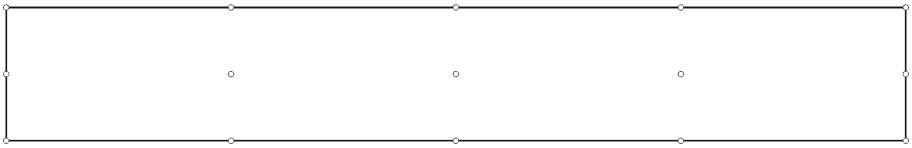

Fig. 3 Node distribution for the meshless moving least-squares method (equally spaced nodes along the bar length L)

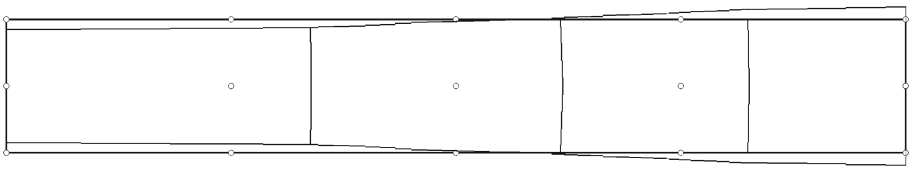

Fig. 4 Bar aspect after deformation

Additionally,

$$p = \frac{F}{2AY_0} \tag{52}$$

$$q = \frac{Ec\,\Theta}{Y_0} \tag{53}$$

For the particular case of $L = 1\,\text{m}$, $A = 0.01\,\text{m}^2$, $F = 5$ MN, $\Theta = 80\,^{\circ}\text{C}$, $E = 200\,\text{GPa}$, $Y_0 = 800\,\text{MPa}$, $c = 14 \times 10^{-6}$, $a = 0.40$ and $b = 0.60$, the analytical solution for the load factor yields $\omega_0 = 2.7137$. Using the current method with a set of 15 nodes (Fig. 3), the approximate solution yielded $\omega = 2.7137$, which corresponds with the analytic solution to the fourth decimal and a residual mean stress of $-13.88\,\text{MPa}$ with a standard deviation of $0.70\,\text{MPa}$. For a mesh formed of rectangular finite elements with 9 velocity nodes and 4 stress nodes, the residual mean stress was $-14.11\,\text{MPa}$ with a null standard deviation [27]. For a mesh composed of triangles with 6 velocity nodes and 3 stress nodes [5], the residual mean stress was $-14.13\,\text{MPa}$ with a standard deviation of $1.97\,\text{MPa}$ [27].

Figure 4 shows a schematic of the deformed bar aspect after the mechanical and thermal loads are applied ($\bar{p} = 0.3125$, $\bar{q} = 0.280$). The obtained numerical result is a velocity field or mechanism, which is shown in Fig. 4 multiplied by an arbitrary time interval to generate a deformation field. In this figure, it can be seen that the bar α is deformed by tension whether bar β is under compression, for the applied loads.

The Bree diagram for this example is shown in Fig. 5. The numerical results are similar to the analytic solution [28] with only a minor difference noted at the points near the interception of the vertical axis. The analytic solution intercepts the vertical axis at $\omega q = 5$. However, for the mixed moving least-squares method, this interception occurs at $\omega q = 4.93$, which corresponds to a maximum error of 1.4 %.

5.2 A cube subjected to a combination of thermal and mechanical loads

Consider the cube, represented schematically in Fig. 6, submitted to a variable pressure, p, together with a thermal variation, Θ.

According to Zouain and Silveira [40], the elastic stresses for this example (Fig. 7) are given by the following:

$$T_x^1 = 0 \qquad T_y^1 = 0 \tag{54}$$

$$T_x^2 = 0 \qquad T_y^2 = -\bar{q} \tag{55}$$

$$T_x^3 = \bar{p} \qquad T_y^3 = \nu\bar{p} - \bar{q} \tag{56}$$

$$T_x^4 = \bar{p} \qquad T_y^4 = \nu\bar{p} \tag{57}$$

where ν represents Poisson's ratio, and q is given by the following:

$$q = E\,c\,\Theta \tag{58}$$

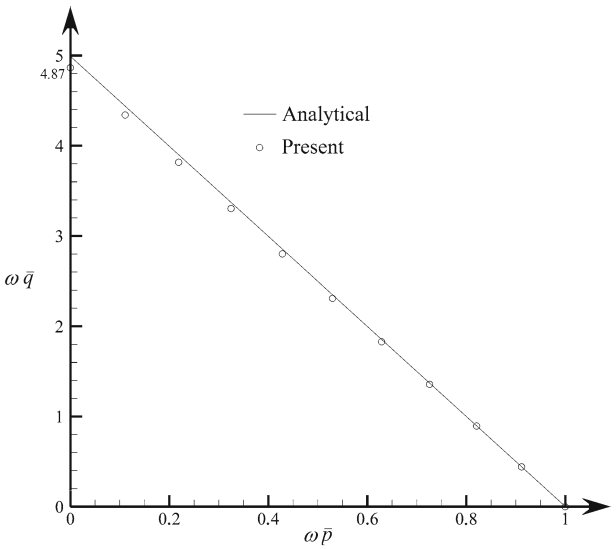

Fig. 5 Bree's diagram for the bar

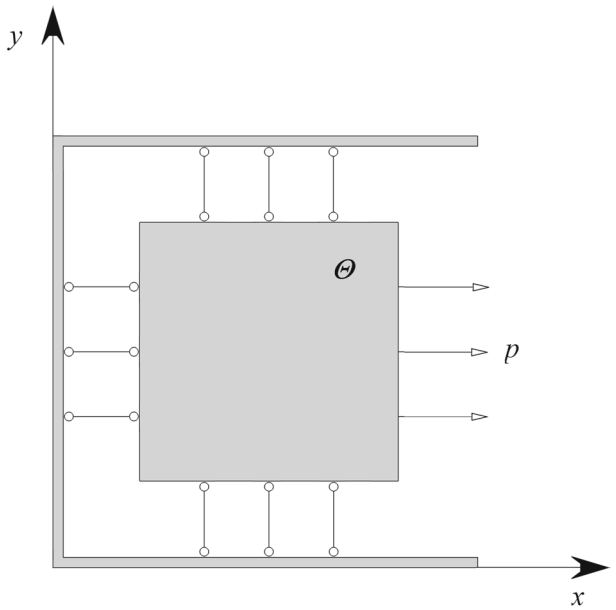

Fig. 6 Cube subjected to a thermo-mechanical load

and $0 \leq p \leq \bar{p}$ and $0 \leq q \leq \bar{q}$.

The value of the load factor is dependent on the determination of the active vertices of the polyhedron of elastic stresses (Fig. 7) [40]. For instance, if vertices 3 and 4 are active, then the analytical load factor is as follows:

$$\omega = \frac{2Y_0}{\sqrt{3\bar{p}^2 + \bar{q}^2}} \tag{59}$$

If the active vertices are 1 and 3, then the load factor becomes the following:

$$\omega = \frac{[(1-2\nu)\,\bar{p} + 2\bar{q}]Y_0}{(1-\nu+\nu^2)\,\bar{p}^2 + \bar{q}^2 + (1-2\nu)\bar{p}\,\bar{q}} \tag{60}$$

For the particular case where the cubes edge measures 1 m, $\bar{p} = 30\,\text{MPa}$, $E = 200\,\text{GPa}$, $c = 14 \times 10^{-6}$, $\Theta = 20°\text{C}$ and $Y_0 = 800\,\text{MPa}$, the analytic solution yields $\omega_0 = 20.9441$. The approximate solution

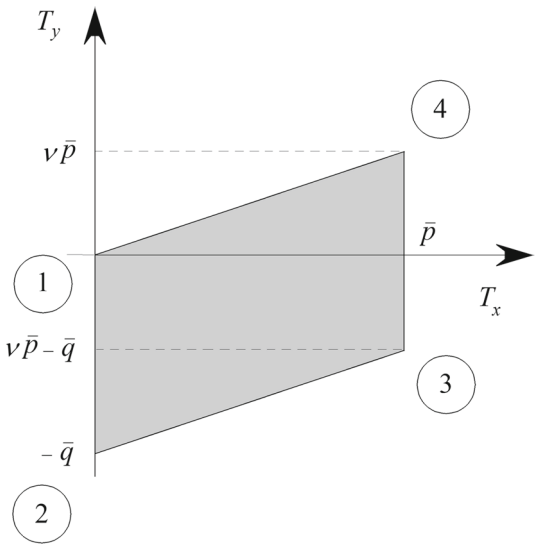

Fig. 7 The elastic stress polyhedron for the cube

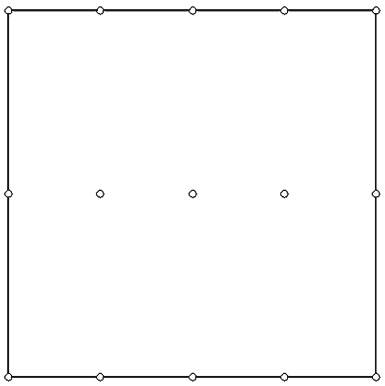

Fig. 8 The face of the cube discretized by nodes

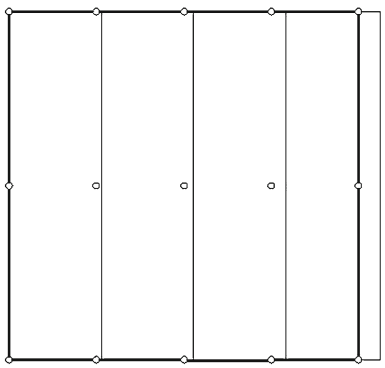

Fig. 9 The cube aspect after deformation

using 15 nodes (Fig. 8) yields $\omega = 20.9441$, which corresponds to the analytic solution to the fourth decimal. The deformation obtained for the cube is shown in Fig. 9.

In this problem, the analytic solution for the residual stress component in the y direction is equal to the yield stress, Y_0, which is 800 MPa for this case. In the x direction, the analytic value of the stress component is zero. The solution obtained using the proposed method is exactly the same as the analytic solution, which

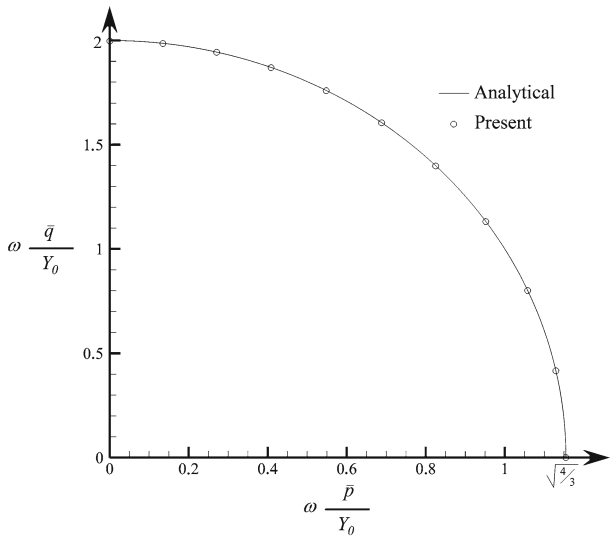

Fig. 10 Bree's diagram of the cube

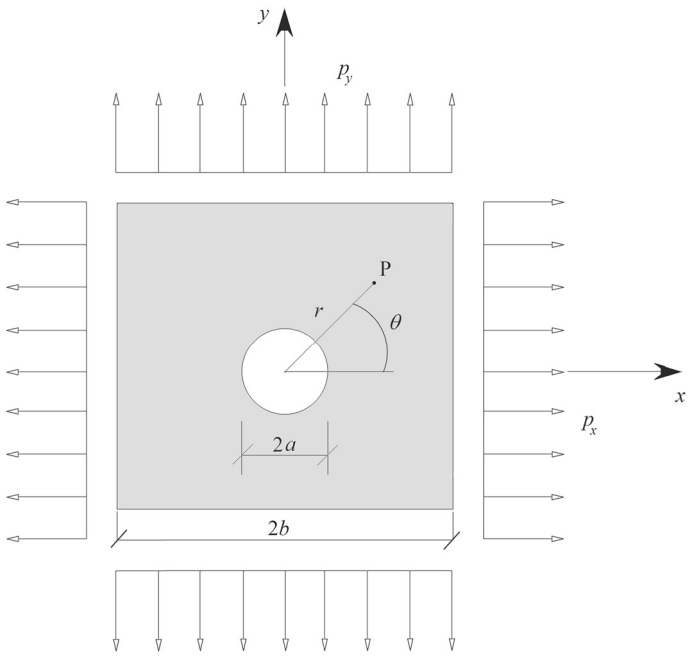

Fig. 11 Square plate subjected to a biaxial effort

is a residual stress of 800 MPa in the y direction and zero in the x direction. The Bree's diagram shown in Fig. 10 coincides with the analytic solution provided by Zouain and Silveira [40].

5.3 A square plate with a central circular hole subjected to a biaxial effort

A square plate with a length of $2b$ and a circular hole with a diameter of $2a$ was subjected to a biaxial effort, as shown in Fig. 11.

The elastic stress, due to the action of p_x on a generic point, P, at a distance, r, from the plate's center is given by the following using polar coordinates [32]:

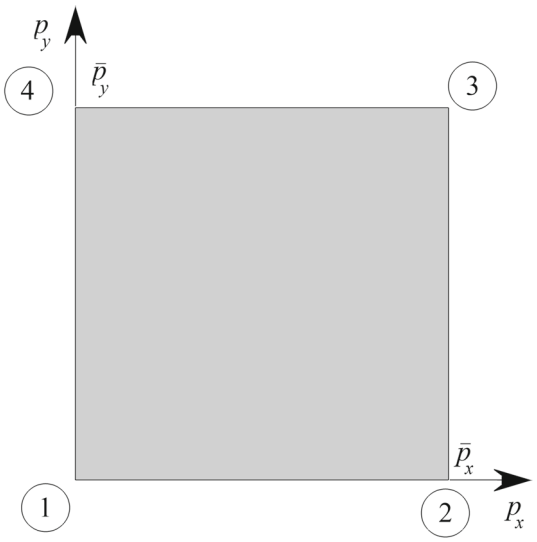

Fig. 12 Polyhedron of acting loads on the plate

$$T_r^{ex} = \frac{p_x}{2}\left(1 - \frac{a^2}{r^2}\right) + \frac{p_x}{2}\left(1 + \frac{3a^4}{r^4} - \frac{4a^2}{r^2}\right)\cos 2\theta \tag{61}$$

$$T_\theta^{ex} = \frac{p_x}{2}\left(1 + \frac{a^2}{r^2}\right) - \frac{p_x}{2}\left(1 + \frac{3a^4}{r^4}\right)\cos 2\theta \tag{62}$$

$$T_{r\theta}^{ex} = -\frac{p_x}{2}\left(1 - \frac{3a^4}{r^4} + \frac{2a^2}{r^2}\right)\sin 2\theta \tag{63}$$

Similarly, the stress due to the action of p_y is as follows:

$$T_r^{ey} = \frac{p_y}{2}\left(1 - \frac{a^2}{r^2}\right) - \frac{p_y}{2}\left(1 + \frac{3a^4}{r^4} - \frac{4a^2}{r^2}\right)\cos 2\theta \tag{64}$$

$$T_\theta^{ey} = \frac{p_y}{2}\left(1 + \frac{a^2}{r^2}\right) + \frac{p_y}{2}\left(1 + \frac{3a^4}{r^4}\right)\cos 2\theta \tag{65}$$

$$T_{r\theta}^{ey} = \frac{p_y}{2}\left(1 - \frac{3a^4}{r^4} + \frac{2a^2}{r^2}\right)\sin 2\theta \tag{66}$$

Assuming that the pressures, p_x and p_y, can vary independently of one another, then the stress polyhedron applied to the plate consists of a rectangle whose vertices are formed by the maximum values of p_x and p_y and where $0 \leq p_x \leq \bar{p}_x$ and $0 \leq p_y \leq \bar{p}_y$, as shown in Fig. 12.

Applying the principle of superposition, the respective components of the stress can be combined to obtain the resulting component for each one of the vertices of the polyhedron loads, as shown in Fig. 12. Therefore, the elastic stress components for each of the vertices can be calculated as follows:

$$T_r^{e1} = 0 \qquad T_\theta^{e1} = 0 \qquad T_{r\theta}^{e1} = 0 \tag{67}$$

$$T_r^{e2} = T_r^{ex} \qquad T_\theta^{e2} = T_\theta^{ex} \qquad T_{r\theta}^{e2} = T_{r\theta}^{ex} \tag{68}$$

$$T_r^{e3} = T_r^{ex} + T_r^{ey} \qquad T_\theta^{e3} = T_\theta^{ex} + T_\theta^{ey} \qquad T_{r\theta}^{e3} = T_{r\theta}^{ex} + T_{r\theta}^{ey} \tag{69}$$

$$T_r^{e4} = T_r^{ey} \qquad T_\theta^{e4} = T_\theta^{ey} \qquad T_{r\theta}^{e4} = T_{r\theta}^{ey} \tag{70}$$

Due to the symmetry of the plate, it is sufficient to investigate a single quadrant, as shown in Fig. 13. Figure 13 also shows the distribution of the 49 nodes used to discretize the plate.

The Bree's diagram for the particular case where $a/b = 0.2$ is shown in Fig. 14. In this figure, the numerical results obtained by the moving least-squares method are compared with the numerical results obtained by

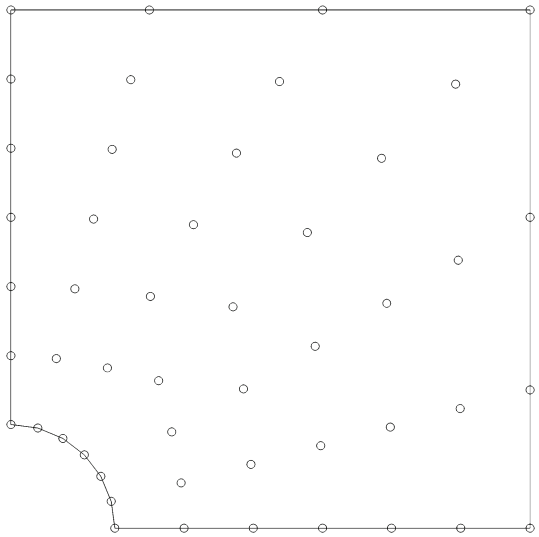

Fig. 13 Distribution of the nodes on a quadrant of the plate

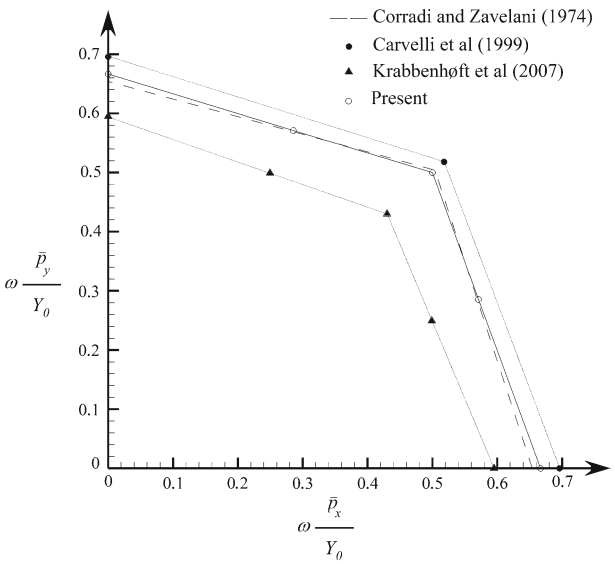

Fig. 14 Bree's diagram for a square plate with a circular central hole

Carvelli et al. [6], Corradi and Zavelani [8] and Krabbenhøft et al. [20]. For the case of a plate made of a material with a yield stress Y_0 and subjected to pressures such that $\bar{p}_x = \bar{p}_y$ (corresponding to the point $\omega\frac{\bar{p}_x}{Y_0} = \omega\frac{\bar{p}_y}{Y_0}$ in Fig. 14), the numerical value given by Corradi and Zavelani [8] is $\omega = 0.504$, for $a/b \to 0.2$, and the analytic value given by Stein et al. [30] is $\omega_0 = 0.50$, for $a/b \to 0$ (not shown in the figure). The load factor calculated by the moving least-squares method is $\omega = 0.49999$, for $a/b \to 0.2$.

Table 1 shows some numerical results for the load factors presented in the literature. The data from Genna [12] and Stein et al. [29] were extracted from graphs using Plot Digitizer [17]. As pointed out by Krabbenhøft et al. [20], a full elastic shakedown procedure would not be necessary as the failure mode is alternating plasticity, for these domains of applied loads. Thus, the accumulated plastic deformation is null, and therefore, there is no mechanism of plastic deformation for a square plate with central circular hole.

Numerical simulations obtained by the moving least-squares method showed coinciding results for the shakedown load factor values, when the number of nodes is increased from 12 to 49, for both uniform and

Table 1 Shakedown load factors for a square plate with central circular hole

Authors	$p_x = p_y$	$p_x = 2p_y$	$p_y = 0$
Belytschko [2]	0.431	0.501	(n/a)
Corradi and Zavelani [8]	0.504	(n/a)	0.654
Genna [12]	0.48	(n/a)	0.65
Stein et al. [29]	0.45	(n/a)	0.62
Gross-Weege [14]	0.446	0.524	0.614
Carvelli et al. [6]	0.518	(n/a)	0.696
Hamadouche [16]	0.490	(n/a)	0.623
Zhang and Raad [37]	0.494	(n/a)	0.574
Zouain et al. [43]	0.429	0.500	0.594
Zhang et al. [38]	0.477	0.549	0.647
Vu et al. [34]	(n/a)	(n/a)	0.599
Liu et al. [22]	0.477	0.549	0.647
Garcea et al. [11]	0.438	0.508	0.604
Krabbenhøft et al. [20]	0.430	0.499	0.595
Tran et al. [33]	0.434	0.505	0.601
Nguyen-Xuan et al. [24]	0.439	0.508	0.601
Present	0.500	0.571	0.667

(n/a) - not available

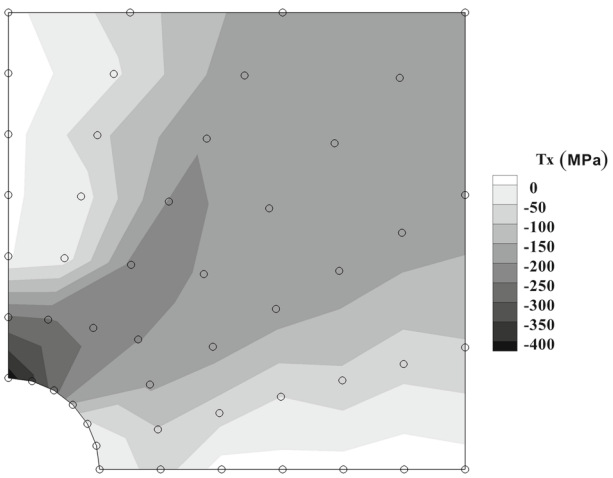

Fig. 15 The distribution of the residual stress component, T_x, obtained by the mixed moving least-squares method, for $\bar{p}_x = 2\bar{p}_y$ and $Y_0 = 600\,\text{MPa}$

nonuniform distribution of nodes. However, there is a considerable variation regarding the quality of the distribution of residual stresses, which is better represented with a finer node distribution.

For $\bar{p}_x = 2\bar{p}_y$, the distribution for the components of the residual stress, T_x, T_y and T_{xy}, obtained by the mixed moving least-squares method is shown in Figs. 15, 16 and 17.

As stated in Sect. 3, the residual stress field is not unique. Figures 15, 16 and 17 present a possible residual stress field that satisfies the Bleich–Melan theorem. In these figures, points close to the hole have higher elastic stresses, as given by Eqs. (61)–(66). Therefore, due to the amplification of the elastic stresses by the shakedown load factor ω, the residual stresses in points within the hole near field are larger than the observed in regions more distant to the center. Moreover, the Bleich–Melan theorem indicates that a residual stress corresponding to a tensile elastic stress is compressive in nature and a residual stress corresponding to a compressive elastic stress is tensile. For the present problem, the domain of load variation shown in Fig. 12 contains only tensile loads and generates a compressive residual stress field as shown in Figs. 15 and 16 for the stress component fields T_x and T_y, respectively, therefore agreeing with the Bleich–Melan theorem statement.

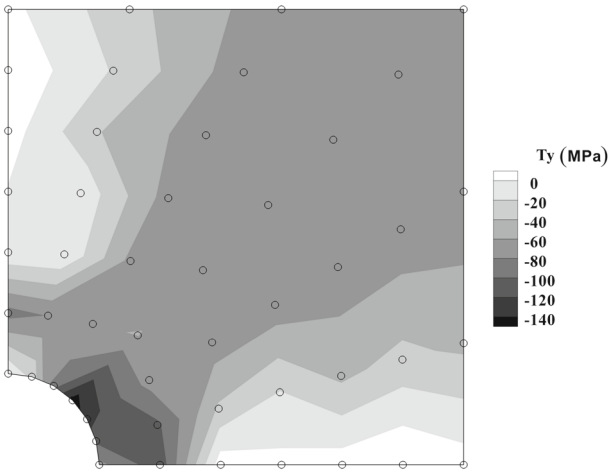

Fig. 16 The distribution of the residual stress component, T_y, obtained by the mixed moving least-squares method for $\bar{p}_x = 2\bar{p}_y$ and $Y_0 = 600\,\text{MPa}$

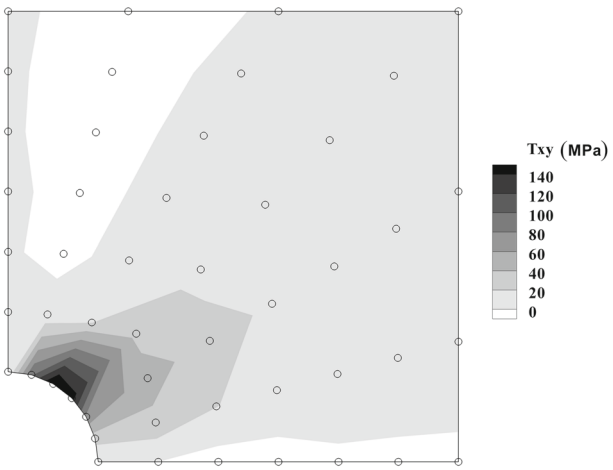

Fig. 17 The distribution of the residual stress component, T_{xy}, obtained by the mixed moving least-squares method for $\bar{p}_x = 2\bar{p}_y$ and $Y_0 = 600\,\text{MPa}$

6 Conclusion

In this paper, a discretization of a mixed variational principle for the elastic shakedown problem using the moving least-squares method is presented. The intrinsic advantage of meshless methods is that there is neither a need to generate a mesh nor establish node connectivity, which reduces the computational implementation burden. Moreover, in the mixed approximation, when the optimization problem is solved, the residual stress and velocity fields are obtained simultaneously, without need for postprocessing calculations.

To validate the proposed procedure, three problems with known analytic solutions were solved. For the analysis of a rectangular sectioned bar subjected to temperature variation and an axial load, the mixed moving least-squares method yielded an accurate approximation for the load factor. The numerical results found for the bar problem are similar to the known analytic solution. For the application of the proposed methodology to a cube subjected to a variable thermal load and constant pressure on its faces, the comparison between numerical and analytical results showed similar agreement. As expected, the analysis of a square plate with a central circular hole under a biaxial uniform load revealed that the collapse occurs due to alternating plasticity and that the solutions obtained for the load factor also coincide with the known analytic values.

Due to the accuracy and ease of computational implementation, the moving least-squares method has shown itself to be a viable alternative to the traditional numerical methods for the elastic shakedown analysis.

References

1. Atluri, S.N., Zhu, T.: New concepts in meshless methods. Int. J. Numer. Methods Eng. **47**, 537–556 (2000)
2. Belytschko, T.: Plane stress shakedown analysis by finite elements. Int. J. Mech. Sci. **14**, 619–625 (1972)
3. Belytschko, T., Lu, Y.Y., Gu, L.: Element-free Galerkin methods. Int. J. Numer. Methods Eng. **37**, 229–256 (1994)
4. Belytschko, T., Krongauz, Y., Organ, D., Fleming, M., Krysl, P.: Meshless methods: an overview and recent developments. Comput. Methods Appl. Mech. Eng. **139**, 3–47 (1996)
5. Borges, L., Zouain, N., Huespe, A.E.: A nonlinear optimization procedure for limit analysis. Eur. J. Mech. A Solids **15**, 487–512 (1996)
6. Carvelli, V., Cen, Z.Z., Liu, Y., Maier, G.: Shakedown analysis of defective pressure vessels by a kinematic approach. Arch. Appl. Mech. **69**, 751–764 (1999)
7. Chen, S., Liu, Y., Cen, J.L.Z.: Performance of the MLPG method for static shakedown analysis for bounded kinematic hardening structures. Eur. J. Mech. A Solids **30**, 183–194 (2011)
8. Corradi, L., Zavelani, A.: A linear programming approach to shakedown analysis of structures. Comput. Methods Appl. Mech. Eng. **3**, 37–53 (1974)
9. Ertz, M., Knothe, K.: Thermal stresses and shakedown in wheel/rail contact. Arch. Appl. Mech. **72**, 715–729 (2003)
10. Fonseca, A.R.: Algoritmos eficientes em métodos sem malha. Tese de D. Sc., Universidade Federal de Minas Gerais, Belo Horizonte Minas Gerais Brasil (2011)
11. Garcea, G., Armentano, G., Petrolo, S., Casciaro, R.: Finite element shakedown analysis of two-dimensional structures. Int. J. Numer. Methods Eng. **63**, 1174–1202 (2005)
12. Genna, F.: A nonlinear inequality, finite element approach to the direct computation of shakedown load safety factors. Int. J. Mech. Sci. **30**(10), 769–789 (1988)
13. Giambanco, F., Palizzolo, L.: Optimal conditions for shakedown design of trusses. Comput. Mech. **16**, 369–378 (1995)
14. Gross-Weege, J.: On the numerical assessment of the safety factor of elastic–plastic structures under variable loading. Int. J. Mech. Sci. **39**(4), 417–433 (1997)
15. Guedes, C.M.C.F.F.M.: Método sem malha em problemas de mecânica computacional. Aplicação a processos de enformação plástica. Tese de D. Sc., Faculdade de Engenharia do Porto, Porto Portugal (2006)
16. Hamadouche, M.A.: Kinematic shakedown by the Norton–Hoff–Friaa regularising method and augmented Lagrangian. C. R. Méc. **330**, 305–311 (2002)
17. Huwaldt, J.A., Steinhorst, S.: Plot digitizer 2.6.6. http://plotdigitizer.sourceforge.net. (2014)
18. Koiter, W.T.: General theorems for elastic plastic solids. In: Sneddon, I.N., Hill, R. (eds.) Progress in Solid Mechanics, vol. 1, pp. 165–221. North-Holland, Amsterdam (1960)
19. König, J.: A method of shakedown analysis of frames and arches. Int. J. Solids Struct. **7**, 327–344 (1971)
20. Krabbenhøft, K., Lyamin, A., Sloan, S.: Bounds to shakedown loads for a class of deviatoric plasticity models. Comput. Mech. **39**, 879–888 (2007)
21. Li, T., Chen, H., Chen, W., Ure, J.: On the shakedown analysis of welded pipes. Int. J. Press. Vessel. Pip. **88**, 301–310 (2011)
22. Liu, Y., Zhang, X., Cen, Z.: Lower bound shakedown analysis by the symmetric Galerkin boundary element method. Int. J. Plast. **21**, 21–42 (2005)
23. Melan, E.: Zur Plastizität des räumlichen Kontinuums. Arch. Appl. Mech. **8**, 116–126 (1938)
24. Nguyen-Xuan, H., Rabczuk, T., Nguyen-Thoi, T., Tran, T.N., Nguyen-Thanh, N.: Computation of limit and shakedown loads using a node-based smoothed finite element method. Int. J. Numer. Methods Eng. **90**, 287–310 (2012)
25. Pham, D.C.: Shakedown limits for reinforced beam structures under fluctuating loads. Int. J. Solids Struct. **36**, 1297–1309 (1999)
26. Ponter, A.R.S., Chen, H.F., Ciavarella, M., Specchia, G.: Shakedown analyses for rolling and sliding contact problems. Int. J. Solids Struct. **43**, 4201–4219 (2006)
27. Ruiz, C.: Adaptação elástica e plástica de materiais com variação na densidade via método dos elementos finitos e métodos sem malha. Tese de D.Sc., COPPE/UFRJ, Rio de Janeiro, RJ, Brasil (2014)
28. Silveira, J.L., Zouain, N.: On extremum principles and algorithms for shakedown analysis. Eur. J. Mech. A Solids **16**(5), 757–778 (1997)
29. Stein, E., Zhang, G., König, J.: Shakedown with nonlinear strain-hardening including structural computation using finite element method. Int. J. Plast. **8**, 1–31 (1992)
30. Stein, E., Zhang, G., Huang, Y.: Modeling and computation of shakedown problems for nonlinear hardening materials. Comput. Methods Appl. Mech. Eng. **103**, 247–272 (1993)
31. Tiel, J.: Convex Analysis: An Introduction Text. Wiley, London (1984)
32. Timoshenko, S.P., Goodier, J.N.: Theory of Elasticity, 3rd edn. McGraw-Hill, New York (1987)
33. Tran, T.N., Liu, G.R., Nguyen-Xuan, H., Nguyen-Thoi, T.: An edge-based smoothed finite element method for primal-dual shakedown analysis of structures. Int. J. Numer. Methods Eng. **82**, 917–938 (2010)
34. Vu, D.K., Yan, A.M., Nguyen-Dang, H.: A dual form for discretized kinematic formulation in shakedown analysis. Int. J. Solids Struct. **41**, 267–277 (2004)
35. Weichert, D., Ponter, A.: A historical view on shakedown theory. In: The History of Theoretical, Material and Computational Mechanics—Mathematics Meets Mechanics and Engineering, Lecture Notes in Applied Mathematics and Mechanics, vol. 1, pp. 169–193. Springer, Berlin (2014)
36. Wu, Z.: Compactly supported positive definite radial functions. Adv. Comput. Math. **4**, 283–292 (1995)
37. Zhang, T., Raad, L.: An eigen-mode method in kinematic shakedown analysis. Int. J. Plast. **18**, 71–90 (2002)
38. Zhang, X., Liu, Y., Cen, Z.: Boundary element methods for lower bound limit and shakedown analysis. Eng. Anal. Bound. Elem. **28**, 905–917 (2004)
39. Zouain, N.: Shakedown and safety assessment. In: Stein, E., de Borst, R., Hughes, T.J.R. (eds.) Encyclopedia of Computational Mechanics, vol. 2, pp. 291–334. Wiley, London (2004)
40. Zouain, N., Silveira, J.L.: Extremum principles for bounds to shakedown loads. Eur. J. Mech. A Solids **18**, 879–901 (1999)

41. Zouain, N., Silveira, J.L.: Variational principles for shakedown analysis. In: Weichert, D., Maier, G. (eds.) Inelastic Analysis of Structures under Variable Loads, pp. 147–165. Kluwer Academic, Dordrecht (2000)
42. Zouain, N., Silveira, J.L.: Bounds to shakedown loads. Int. J. Solids Struct. **38**, 2249–2266 (2001)
43. Zouain, N., Borges, L., Silveira, J.L.: An algorithm for shakedown analysis with nonlinear yield functions. Comput. Methods Appl. Mech. Eng. **191**, 2463–2481 (2002)